Room-Temperature All-Semiconducting Sub-10-nm Graphene Nanoribbon Field-Effect Transistors

Xinran Wang,[1] Yijian Ouyang,[2] Xiaolin Li,[1] Hailiang Wang,[1] Jing Guo,[2] and Hongjie Dai[1,*]

[1]*Department of Chemistry and Laboratory for Advanced Materials, Stanford University, Stanford, California 94305, USA*
[2]*Department of Electrical and Computer Engineering, University of Florida, Gainesville, Florida 32611, USA*

(Received 21 March 2008; published 20 May 2008)

Sub-10 nm wide graphene nanoribbon field-effect transistors (GNRFETs) are studied systematically. All sub-10 nm GNRs afforded semiconducting FETs without exception, with I_{on}/I_{off} ratio up to 10^6 and on-state current density as high as $\sim$2000 μA/μm. We estimated carrier mobility $\sim$200 cm^2/V s and scattering mean free path $\sim$10 nm in sub-10 nm GNRs. Scattering mechanisms by edges, acoustic phonon, and defects are discussed. The sub-10 nm GNRFETs are comparable to small diameter ($d \leq \sim$1.2 nm) carbon nanotube FETs with Pd contacts in on-state current density and I_{on}/I_{off} ratio, but have the advantage of producing all-semiconducting devices.

DOI: 10.1103/PhysRevLett.100.206803 PACS numbers: 85.35.−p, 73.63.−b

Graphene-based electronics has attracted much attention due to high carrier mobility in bulk graphene [1–5]. For mainstream logic applications, graphene width confinement down to sub-10 nm is needed to open sufficient band gap for room temperature transistor operation. Although sub-10 nm graphene nanoribbon (GNR) was predicted to be semiconducting by several theories [6–10], experimental work in this area [11,12] has been scarce partly due to challenges in patterning GNR below 20 nm by plasma etching. Recently, sub-10 nm GNRs with smooth edges were obtained and demonstrated to be semiconductors with band gap inversely proportional to w (Ref. [13]). Various fundamental questions remain to be addressed such as the performance limit of graphene nanoribbon field-effect transistors (GNRFETs), the intrinsic carrier mobility in narrow ribbons, and comparison of GNRs with other materials including carbon nanotubes (CNTs).

In this work, we studied both sub-10-nm GNRs and wide GNRs ($w \sim$ 10–60 nm). All the sub-10-nm GNRs (a total of $\sim$40) were found semiconducting with adequate band gap for transistor operation at room temperature. The GNR synthesis and transistor fabrication process (see supplementary material [14]) were similar to that described in Ref. [13]. Figures 1(b) and 1(c) show atomic force microscopy (AFM) images of typical sub-10-nm ($w \sim 2 \pm 0.5$ nm) and wide ($w \sim 60 \pm 5$ nm) GNR devices. We carefully used AFM to measure the width (with careful tip size correction), lengths, and number of layers of our GNR devices. Only a few discrete heights have been observed for all the GNR samples we made, i.e., $\sim$1.1, 1.5, and 1.9 nm, which were assigned as one-, two-, and three-layer graphene [12,13]. All of the devices presented in this Letter show a height of $\sim$1.5 nm and are assigned as two-layer GNRs, unless stated otherwise. We also carried out confocal surface enhanced Raman spectroscopy study on GNR devices. All the details and results are described in supplementary information [14].

Since our GNRFETs were Schottky barrier (SB) type FETs where the current was modulated by carrier tunneling probability through SB at contacts, high work function metal Pd was used to minimize the SB height for holes in p type transistors. In fact we used Ti/Au as contact and found that Pd did give higher I_{on} in device with similar dimensions. 10 nm SiO_2 gate dielectrics was also important to achieve higher I_{on} because it significantly reduced SB width at contacts compared to 300 nm in previous work [13]. Figures 2(a) and 2(b) showed the transfer

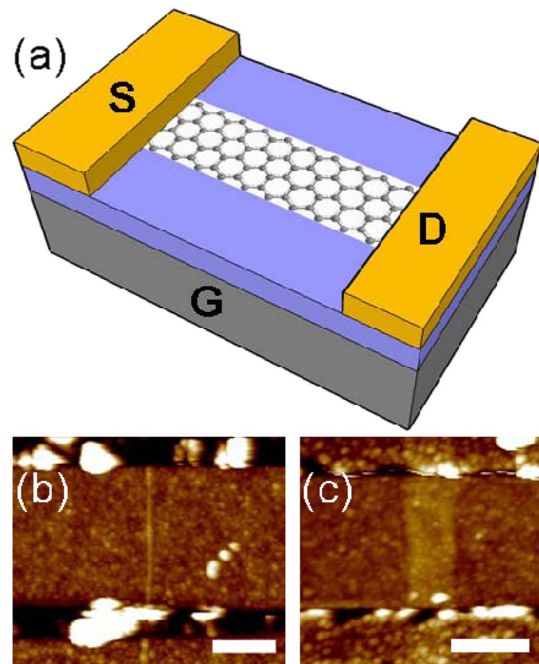

FIG. 1 (color online). GNRFET device images. (a) Schematics of GNRFETs on 10 nm SiO_2 with Pd S/D. P^{++} Si is used as backgate. (b) AFM image of a $w \sim 2 \pm 0.5$ nm, $L \sim 236$ nm GNRFET. Scale bar is 100 nm. (c) AFM image of a $w \sim 60 \pm 5$ nm, $L \sim 190$ nm wide GNR device. Scale bar is 100 nm.

 © 2008 The American Physical Society

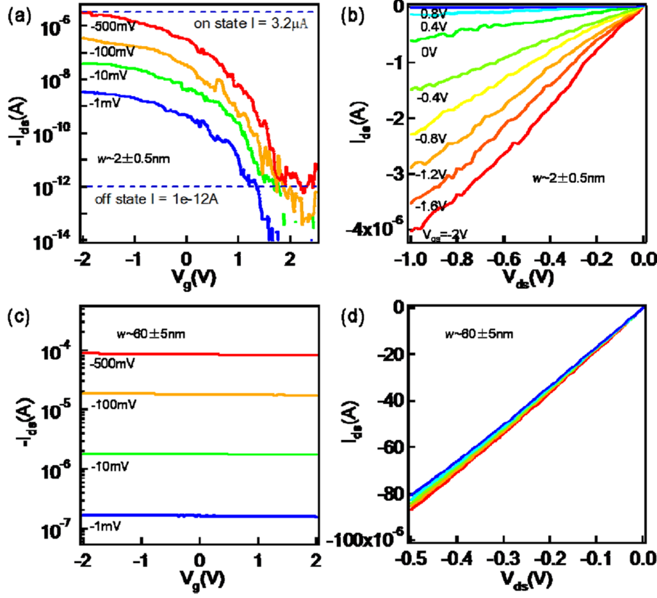

FIG. 2 (color online). Transistor performance of GNRFETs. (a) Transfer characteristics (current vs gate voltage $I_{ds} - V_{gs}$) under various V_{ds} for the device shown in Fig. 1(b). I_{on}/I_{off} ratio of $>10^6$ is achieved at room temperature. (b) Output characteristics ($I_{ds} - V_{ds}$) under various V_{gs} for the device shown in Fig. 1(b). On current density is $\sim 2000\ \mu\text{A}/\mu\text{m}$ in this device. (c) Transfer and (d) output characteristics of the device shown in Fig. 1(c).

and output characteristics for the $w \sim 2 \pm 0.5$ nm $L \sim 236$ nm GNR device shown in Fig. 1(b). This device delivered $I_{on} \sim 4\ \mu$A ($\sim 2000\ \mu\text{A}/\mu\text{m}$) at $V_{ds} = 1$ V, I_{on}/I_{off} ratio $>10^6$ at $V_{ds} = 0.5$ V, subthreshold slope ~ 210 mV/decade and transconductance $\sim 1.8\ \mu$S ($\sim 900\ \mu\text{S}/\mu\text{m}$). For wide GNR devices, they all showed metallic behavior because of vanishingly small band gaps [Figs. 2(c) and 2(d)]. Compared to sub-10 nm GNRFETs with similar channel length, the current density in wide GNR devices was usually higher [$\sim 3000\ \mu\text{A}/\mu\text{m}$ at $V_{ds} = 1$ V for the device in Fig. 2(d)]. We note that our wide GNRs showed relatively weak gate dependence in transfer characteristics, likely due to interaction between layers [12]. The Dirac point was usually not observed around zero gate bias, indicating p-doping effects at the edges or by physisorbed species during the chemical treatment steps [15].

To investigate the intrinsic properties of GNRs such as carrier scattering mean free path (MFP) and mobility, we made different channel length transistors on the same GNR. Figure 3(a) showed an AFM image of a typical $w \sim 2.5 \pm 1$ nm GNR with $L \sim 110$, 216, and 470 nm segments that delivered $I_{on} \sim 5$, ~ 4, and $\sim 2\ \mu$A, respectively [only the output characteristics of the upper segment is shown in Fig. 3(b)]. We measured the low bias resistance R_{tot} of the three segments [Fig. 3(c)], and extrapolated the parasitic contact resistance $R_c = \sim 60\ \text{k}\Omega$ for this device.

Under low bias, the on-state resistance in GNR due to scattering can be written as

$$R = R_{tot} - R_c = \left(\frac{h}{2e^2}\right)\left(\frac{L}{\lambda}\right) = L\left(\frac{1}{\lambda_{edge}} + \frac{1}{\lambda_{ap}} + \frac{1}{\lambda_{defect}}\right)\left(\frac{h}{2e^2}\right), \tag{1}$$

where L is channel lengths, λ is total scattering MFP, and λ_{edge}, λ_{ap}, λ_{defect} denote MFP due to GNR edge, acoustic phonon, and defect scattering, respectively. The scattering MFP of GNR

$$\lambda = L\left(\frac{h}{2e^2}\right)/(R_{tot} - R_c). \tag{2}$$

We estimated $\lambda \sim 14$, 11, and 12 nm in the three segments of the GNR. Based on standard transistor model, the intrinsic carrier mobility is

$$\mu = \frac{g_m L}{C_{gs} V_{ds}}, \tag{3}$$

where $g_m = \frac{dI_{ds}}{dV_{gs}}|V_{ds}$ is the intrinsic transconductance obtained from the measured g_m^{mes} by excluding the source resistance $g_m = g_m^{mes}/(1 - g_m^{mes} R_s)$ and C_{gs} is gate capacitance per unit length. We used three-dimensional electrostatic simulation to calculate C_{gs} (see supplementary information [14]) and obtained $C_{gs} \sim 26$ pF/m for a $w \sim 2.5$ nm ribbon. Using Eq. (3), we calculated $\mu \sim 174$, 171, and 189 $\text{cm}^2/\text{V s}$ in the three segments after excluding the effects of contact resistance. Figure 3(b) compares the computed I_{ds} vs V_{ds} characteristics by using a square law model in series with the parasitic resistance to the experimental data for the 470 nm GNRFETs.

In narrow GNRs, edge may play an important role. When electrons travel to an edge, a scattering event happens if the edge is not perfect. The edge scattering MFP is modeled as (see supplementary information [14])

$$\lambda_{edge} = \frac{1}{P}\frac{k_{\parallel}}{k_{\perp}} w = \frac{w}{P}\sqrt{\left(1 + \frac{E_k}{\Delta}\right)^2 - 1}, \tag{4}$$

where $k_{\parallel}$ and $k_{\perp}$ are k-space wave vectors along and perpendicular to the GNR direction, E_k is the kinetic energy of electrons, Δ is half band-gap energy, and P is the probability of backscattering which depends on edge quality. From experiment, our low field $\lambda \approx 12$ nm $< \lambda_{edge}$, suggesting a backscattering probability $P < 20\%$ for this ribbon. Assuming similar edge quality in various widths GNRs, our model predicts that λ_{edge} is proportional to w. Experimentally, we fabricated multiple channel length GNRFETs with different width ribbons and observed the trend that wider sub-10-nm GNRs tent to have

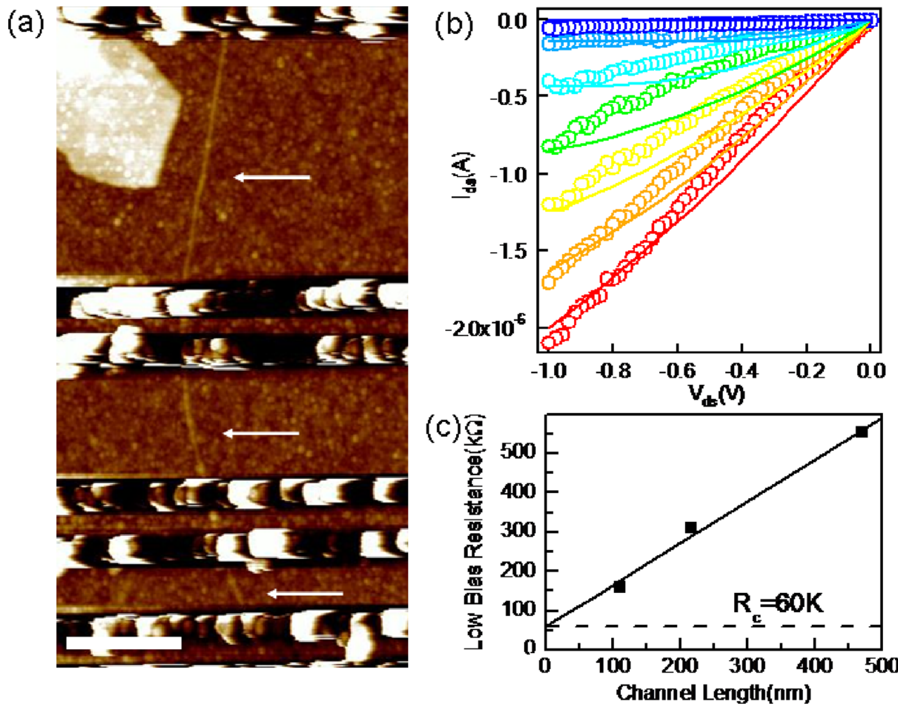

FIG. 3 (color online). Three channel lengths GNRFET. (a) AFM image of a typical $w \sim 2.5 \pm 1$ nm GNRFETs with three channel lengths. White arrows are pointing to the channels. $L \sim 110$, 216, and 470 nm for the lower, middle, and upper segments, respectively. Scale bar is 200 nm. (b) Output characteristics (symbols) and simulations (lines) for the upper segment ($L \sim 470$ nm) of the device in (a). From bottom, V_{gs} is from -2 to 0.4 V, with 0.4 V/step. (c) Measured low bias on-state resistance (symbols) and linear fit (line) of the three segments in (a). The extrapolated $R_c \approx$ 60 kΩ.

higher mobility [Fig. 4(a), data obtained from multiprobe measurements excluding contact resistance] and MFP, although there were some device-dependent fluctuations. Acoustic phonon and defect scattering can also be responsible for the short MFP. Although $\lambda_{\mathrm{ap}} \sim 10\ \mu$m is predicted for a $w \sim 2.5$ nm hydrogen terminated zigzag GNR [16], we expect it shorter in our GNRs since the edge is probably not perfect due to possibly mixed edge shape and dangling bonds [13]. At high bias ($V_{ds} = 1$ V), λ_{edge} is longer than low bias, in this case, it is possible that optical phonon scattering limits the total MFP, with $\lambda_{\mathrm{op}} \sim 10$ nm [16], similar to CNTs.

We next analyze how close the GNRFET operates to the ballistic performance limits by comparing experiments with theoretical modeling. The theoretical model computes the ballistic performance limits by assuming a single ballistic channel and ideal contacts (sufficiently negative SBs) [17]. We found that the $L \sim 236$ nm device in Figs. 2(a) and 2(b) delivered about 21% of the ballistic current at $V_{ds} = 1$ V, and about 4.5% of the ballistic current at low $V_{ds} < 0.1$ V. The highest high bias ballisticity in our studied devices is $\sim$38%. The ballisticity at low drain bias is consistent with the short edge elastic scattering MFP, but the large ballisticity at high drain biases is

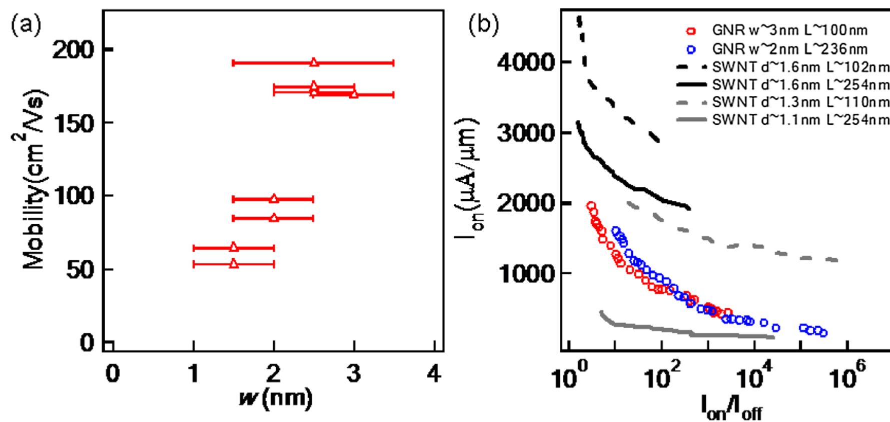

FIG. 4 (color online). GNRFETs and CNTFETs performance comparison. (a) Mobility vs w for multichannel GNRFETs. All data here were obtained from multiprobe measurements of single ribbons to exclude contact resistance. (b) Current density (current normalized by w for GNRs, $2d$ for CNTs) as a function of $I_{\mathrm{on}}/I_{\mathrm{off}}$ under $V_{dd} = V_{ds} = 0.5$ V and $V_{gs}(\mathrm{on}) - V_{gs}(\mathrm{off}) = 2$ V. Red (or gray) symbol: $w \sim 3$ nm $L \sim 100$ nm GNR; blue (or dark gray) symbol: $w \sim 2$ nm $L \sim 236$ nm GNR; black dashed line: $d \sim 1.6$ nm $L \sim 102$ nm CNT; black solid line: $d \sim 1.6$ nm $L \sim 254$ nm CNT; gray dashed line: $d \sim 1.3$ nm $L \sim 110$ nm CNT; gray solid line: $d \sim 1.1$ nm $L \sim 254$ nm CNT.

surprising, especially considering that optical phonon (OP) or zone boundary phonon (ZBP) emission, which has a MFP of ~10 nm, exists at high drain biases. The reasons could be similar to the small direct effect of OP scattering on the current in CNTFETs [18]. Because the OP/ZBP energy is high (~0.2 eV), a carrier backscattered by emitting an OP/ZBP does not have enough energy to overcome the barrier near the source end of the channel, and return back to the source. Any subsequent edge scattering after OP/ZBP emission has a small direct effect on the DC current because edge scattering is elastic and does not change the carrier energy. Such a carrier rattles around in the channel and finally diffuses out of the drain. At high drain biases, therefore, only elastic scattering near the beginning of the channel matters and the rest of the channel essentially operates as a carrier absorber.

Compared to the earlier works on GNR of 20 nm width [19], the devices in the current work show 10^5 higher I_{on}/I_{off} ratio at room temperature, ~20 times higher on current density (at $V_{ds} = 1$ V) and ~100 times higher transconductance per μm, due to larger band gaps, high GNR quality with better edge smoothness [13], thin gate oxide, and short GNR channel. At the same carrier concentration (e.g., $V_g = -0.67$ V, corresponding to -20 V on 300 nm SiO_2) and $V_{ds} = 1$ V, our wide GNR devices deliver higher current density (~2000–3000 $\mu A/\mu m$) than previously reported bilayer GNR with similar width (~50 $\mu A/\mu m$) [12]. After correction for ~10 times channel lengths difference, our current levels are still a few times higher, indicating good GNR quality.

To further access the performance of our GNRFETs, we compared with CNTFETs. We fabricated Pd contacted CNTFETs on 10 nm SiO_2 with similar channel lengths. The performances of our CNTFETs (I_{on} and I_{on}/I_{off} ratio) are very similar to previously published results [20]. We compared the on current density with different diameter CNTs at the same power supply voltage $V_{dd} = V_{ds} = 0.5$ V and I_{on}/I_{off} ratio [21]. We used $V_{gs}(\text{on}) - V_{gs}(\text{off}) = 2$ V, equivalent to a 10 nm gate dielectrics with dielectric constant $\varepsilon \approx 4 \times 3.9 = 15.6$. In Fig. 4(b), we plotted two representative GNRFETs with $w \sim 3$ nm, $L \sim 100$ nm and $w \sim 2$ nm, $L \sim 236$ nm, and compared them with $d \sim 1.6$ nm, 1.3 nm, and 1.1 nm CNTFETs with similar channel lengths. Both GNRs have on current density ~2000 $\mu A/\mu m$. The $d \sim 1.6$ nm CNTs outperform GNRs in terms of on current density (>3000 $\mu A/\mu m$) but exhibit high off state leakage and a maximum I_{on}/I_{off} ratio $<10^3$. For $d \sim 1.3$ nm CNTs, they outperform GNRs in current density at the same I_{on}/I_{off} ratio [Fig. 4(b)]. The $d \sim 1.1$ nm CNTs, on the other hand, deliver much lower current density than GNRs at the same I_{on}/I_{off} ratio, probably due to large positive SB, short AP MFP [22], and defects [23].

Our sub-10-nm GNRFETs afford all-semiconducting nanoscale transistors that are comparable in performance to small diameter carbon nanotube devices. GNRs are possible candidates for future nanoelectronics. Future work should focus on elucidating the atomic structures of the edges of our GNRs and correlate with the performances of GNRFETs. The integration of ultrathin high-κ dielectrics [24] and more aggressive channel length scaling is also needed to achieve better electrostatics, higher I_{on}, and ideal subthreshold slope.

This work was supported in part by MARCO MSD Focus Center and Intel.

*To whom all correspondence should be addressed. hdai@stanford.edu

[1] A. K. Geim and K. S. Novoselov, Nat. Mater. **6**, 183 (2007).
[2] K. S. Novoselov *et al.*, Science **306**, 666 (2004).
[3] Y. Zhang, Y.-W. Tan, H. L. Stormer, and P. Kim, Nature (London) **438**, 201 (2005).
[4] K. S. Novoselov *et al.*, Nature (London) **438**, 197 (2005).
[5] C. Berger *et al.*, Science **312**, 1191 (2006).
[6] K. Nakada, M. Fujita, G. Dresselhaus, and M. S. Dresselhaus, Phys. Rev. B **54**, 17 954 (1996).
[7] K. Wakabayashi, Phys. Rev. B **64**, 125428 (2001).
[8] Y.-W. Son, M. L. Cohen, and S. G. Louie, Phys. Rev. Lett. **97**, 216803 (2006).
[9] L. Yang *et al.*, Phys. Rev. Lett. **99**, 186801 (2007).
[10] V. Barone, O. Hod, and G. E. Scuseria, Nano Lett. **6**, 2748 (2006).
[11] M. Y. Han, B. Ozyilmaz, Y. Zhang, and P. Kim, Phys. Rev. Lett. **98**, 206805 (2007).
[12] Y.-M. Lin and P. Arouris, Nano Lett. (to be published).
[13] X. Li *et al.*, Science **319**, 1229 (2008).
[14] See EPAPS Document No. E-PRLTAO-100-074821 for supplementary material. For more information on EPAPS, see http://www.aip.org/pubservs/epaps.html.
[15] J. Moser, A. Barreiro, and A. Bachtold, Appl. Phys. Lett. **91**, 163513 (2007).
[16] D. Gunlycke, H. M. Lawler, and C. T. White, Phys. Rev. B **75**, 085418 (2007).
[17] M. S. Lundstrom and J. Guo, *Nanoscale Transistors: Device Physics, Modeling, and Simulation* (Springer, New York, NY, 2006).
[18] A. Javey *et al.*, Nano Lett. **4**, 1319 (2004).
[19] Z. Chen *et al.*, Physica (Amsterdam) **40E**, 228 (2007).
[20] W. Kim *et al.*, Appl. Phys. Lett. **87**, 173101 (2005).
[21] A. Javey *et al.*, Nano Lett. **5**, 345 (2005).
[22] G. Pennington and N. Goldsman, Phys. Rev. B **71**, 205318 (2005).
[23] B. C. Pan, W. S. Yang, and Jinlong Yang, Phys. Rev. B **62**, 12652 (2000).
[24] B. Ozyilmaz, P. Jarillo-Herrero, D. Efetov, and P. Kim, Appl. Phys. Lett. **91**, 192107 (2007).